HHS Public Access

Author manuscript

Biol Psychiatry Cogn Neurosci Neuroimaging. Author manuscript; available in PMC 2024 January 01.

Published in final edited form as:

Biol Psychiatry Cogn Neurosci Neuroimaging. 2023 January ; 8(1): 79–90. doi:10.1016/j.bpsc.2021.11.008.

A Comprehensive Analysis of Cerebellar Volumes in the 22Q11.2 Deletion Syndrome

J. Eric Schmitt[1,2,*], **John J. DeBevits**[2], **David R. Roalf**[1], **Kosha Ruparel**[1], **R. Sean Gallagher**[1], **Ruben C. Gur**[1], **Aaron Alexander-Bloch**[1], **Tae-Yeon Eom**[3], **Shahinur Alam**[4], **Jeffrey Steinberg**[4], **Walter Akers**[4], **Khaled Khairy**[5], **T. Blaine Crowley**[6], **Beverly Emanuel**[6,7], **Stanislav Zakharenko**[3], **Donna McDonald-McGinn**[6,7], **Raquel E. Gur**[1,2]

[1]Brain Behavior Laboratory, Department of Psychiatry, Neurodevelopment and Psychosis Section, University of Pennsylvania, Philadelphia, PA 19104, USA.

[2]Department of Radiology, Division of Neuroradiology, Hospital of the University of Pennsylvania, Philadelphia, PA 19104, USA.

[3]Department of Developmental Neurobiology, St. Jude Children's Research Hospital, Memphis, TN 38105, USA.

[4]Center for Bioimage Informatics, St. Jude Children's Research Hospital, Memphis, TN 38105, USA

[5]Center for In Vivo Imaging and Therapeutics, St. Jude Children's Research Hospital, Memphis, TN 38105, USA.

[6]Division of Human Genetics, Children's Hospital of Philadelphia, Philadelphia, PA 19104, USA.

[7]Department of Pediatrics, Perelman School of Medicine, University of Pennsylvania, Philadelphia, PA 19104, USA.

Abstract

Background: The presence of a 22q11.2 microdeletion (22q11DS) ranks among the greatest known genetic risk factors for the development of psychotic disorders. There is emerging evidence that the cerebellum is important in the pathophysiology of psychosis. However, there is currently imited information on cerebellar neuroanatomy in 22q11DS specifically.

Methods: High-resolution 3T MRI was acquired in seventy-nine individuals with 22q11DS and seventy typically developing (TD) controls (N=149). Lobar and lobule-level cerebellar volumes were estimated using validated automated segmentation algorithms, and subsequently group differences were compared. Hierarchical clustering, principal component analysis, and

[*]Corresponding Author: Departments of Radiology and Psychiatry Hospital of the University of Pennsylvania 3400 Spruce Street, Philadelphia, Pennsylvania 19104, Telephone: 215-662-6892, Fax: 215-662-3283, eric.schmitt@stanfordalumni.org.

Disclosures: All authors report no biomedical financial interests or potential conflicts of interest.

graph theoretical models were used to explore inter-cerebellar relationships. Cerebro-cerebellar structural connectivity with cortical thickness was examined via linear regression models.

Results: Individuals with 22q11DS had, on average, 17.3% smaller total cerebellar volumes relative to TD (p-value<0.0001). The lobules of the superior posterior cerebellum (e.g. VII and VIII) were particularly affected in 22q11DS. However, all cerebellar lobules were significantly smaller, even after adjusting for total brain volumes (all cerebellar lobule p-values <0.0002). The superior posterior lobule (SPL) was disproportionately associated with cortical thickness in the frontal lobes and cingulate cortex, brain regions known be affected in 22q11DS. Exploratory analyses suggested that SPL, particularly Crus I, may be associated with psychotic symptoms in 22q11DS.

Conclusions: The cerebellum is a critical but understudied component of the 22q11DS neuroendophenotype.

Keywords

22q11.2 deletion syndrome; cerebellum; Crus I; psychosis; MRI; genetics; schizophrenia

Introduction:

Schizophrenia is a devastating psychiatric disease characterized by a spectrum of symptoms including disorganized thinking, hallucinations, delusions, and cognitive deficits. The genetic contributions to schizophrenia are among the highest of all mental disorders, with an estimated heritability approaching 80% (1). Most genetic variants associated with schizophrenia have relatively small effect sizes (2–4). However, the copy number variant at 22q11.2 confers an ~30% lifetime risk of schizophrenia (~20–30 times the general population) and ~50% risk of psychosis(5–7). The 22q11.2 deletion syndrome (22q11DS) also increases liability to several other mental disorders, particularly autism spectrum disorders (ASD) and attention deficit hyperactivity disorder (ADHD) (8).

For over two decades, neuroimaging studies have characterized the 22q11DS neuroendophenotype, in search of genetically-mediated neural substrates of psychosis (9–16). Prior studies have found relatively consistent reductions in cerebral, hippocampal, and subcortical brain volumes, as well as widespread reductions in cerebral surface area, increased cortical thickness, and disrupted cortico-cortical connectivity when compared to typically developing (TD) controls (11, 12, 14, 17–19). Several brain regions that are particularly impacted in 22q11DS (e.g. superior temporal gyrus, hippocampus) are also implicated in the pathophysiology of schizophrenia (16, 20, 21).

The cerebellum has historically been overlooked in neuropsychiatric studies, traditionally considered responsible only for the coordination of motor activity. However, there is emerging evidence that the cerebellum is critical to both cognition and affect (22–25). Mirroring the more well-established motor dysmetria associated with cerebellar injury, the cognitive symptoms associated with cerebellar injury have been termed “dysmetria of thought” – an inability to coordinate higher brain functions (23). Cerebellar anomalies have

been implicated in several psychiatric diseases, including schizophrenia, autism, and ADHD (26, 27).

Yet to our knowledge, there are only two prior studies that investigated regional cerebellar substructure in 22q11DS; both focused solely on mid-sagittal regions of interest (ROIs). Eliez et al. manually measured vermian area (3 ROIs: lobules I–V, VI–VII, and VIII–X) in 24 individuals with 22q11DS and 24 matched controls (28). They found a significant 16.6% reduction in lobules VI-VII in subjects with 22q11DS, and nonsignificant decreases elsewhere (7.0% for lobules I-V, and 17.3% for VIII-X). Similarly, Bish et al. measured mid-sagittal area via analogous manual tracings in 31 participants with 22q11DS (29). Smaller vermian area was observed in 22q11DS relative to the TD group, including a statistically significant 15.7% reduction in lobules I-V (anterior lobe) after adjusting for total brain volume. Nonsignificant smaller volumes in 22q11DS were observed in both superior posterior (16.1%) and the inferior posterior (19.3%) vermian ROIs.

The principal aim of the current study was to perform a systematic survey of regional cerebellar volumes in 22q11DS using high field strength MRI, a large sample, and validated image processing algorithms. Based on prior work on vermis and the potential role of the superior posterior cerebellum in cognition (22), we hypothesized that in addition to global cerebellar reductions, we would observe disproportionate reductions in lobules within the superior posterior lobe(28). We also explored cerebello-cerebellar relationships using several different multivariate perspectives, namely hierarchical cluster analysis, principal components analysis, and graph theoretical models. Given prior evidence of disrupted structural connectivity in the cerebrum (11, 30, 31), we expected to observe weakened network cohesion in the cerebellum in 22q11DS. We additionally examined relationships between our novel cerebellar measures and the more well-established 22q11DS supratentorial endophenotype, via analyses of cerebro-cerebellar structural connectivity. Given the presence of well-established, regionally-specific cerebro-cerebellar pathways (32), we hypothesized that neuroanatomic variation in cerebellar architecture would be associated with those regions of the cerebral cortex that have already been implicated in 22q11DS (12, 15, 16). Finally, we performed exploratory analysis investigating associations between psychosis and cerebellar anatomy in 22q11DS.

Methods and Materials:

Sample and Data Acquisition:

Data were obtained via the prospective study *Brain-Behavior and Genetic Studies of the 22q11DS* performed at the University of Pennsylvania and the Children's Hospital of Philadelphia. This study has been described in detail elsewhere (16). Briefly, inclusion criteria were age >8 years, intelligence quotient (IQ) >70, and sufficient clinical stability to tolerate MRI (as determined by a multidisciplinary clinical research team); participants were excluded if they had IQ<70 or serious neurological disorders (e.g. uncontrolled seizures, head trauma). Deletion status was confirmed using multiplex ligation-dependent probe amplification (33); most subjects (91%) carried the common A-D deletion. Seventy-nine subjects with 22q11DS were included. Psychopathology was assessed with the Structured Interview for Prodromal Syndromes (SIPS) (34), the Schedule for Affective Disorders

and Schizophrenia for School Age Children (K-SADS) (35), and the psychotic and mood differential diagnosis modules of the Structured Clinical Interview for DSM-IV (SCID) (36); additional details on the behavioral assessment protocols can be found in Tang et al. (37).

Seventy non-deleted, typically developing (TD) control subjects were obtained from the Philadelphia Neurodevelopmental Cohort (PNC), a large prospective study using the identical scanner and imaging protocols (38). Table 1 summarizes the demographic characteristics of the samples. There was a statistically significant group difference in scan age, driven by a few outliers in the 22q11DS group; group differences in scan age were therefore partially corrected statistically. We also repeated our analyses with a more closely age-matched subset of the data (Supplementary Data), with similar results to those presented here.

Image Acquisition/Processing:

High-resolution MRI was acquired using a 3T scanner (TIM Trio; Siemens, Erlangen, Germany) and 32-channel head coil. T1-weighted magnetization prepared rapid acquisition gradient echo (MP-RAGE) data was acquired with the following parameters; TR/TE 1810/3.51ms; inversion time 1100ms; FOV=180×240mm; effective resolution $1mm^3$. Images were imported into the CIVET pipeline (v2–1-1) for automated skull stripping, non-uniformity correction, and to estimate total brain volume (39–41). After visual inspection, cerebellar segmentation was performed using Multiple Automatically Generated Templates (MAGeT), an automated, multi-atlas cerebellar parcellation algorithm (42, 43). MAGeT estimates cerebellar volumes based on five high-resolution MRI atlases (3 female, 2 male), with each atlas defined by 2 trained anatomists blinded to each other's work. The algorithm first transforms each atlas to a subset of the sample (21 randomly selected subjects) via nonlinear registration in order to generate a template library (5×21 = 105 templates). This step is advantageous in that it helps account for individual variation in cerebellar morphology, and subsequently improves image registration. A second nonlinear registration step was then performed to propagate ROIs between templates and individual subjects. Lobule-level ROIs for each subject were then automatically generated by assigning each voxel to the ROI that was most frequently observed at that voxel location (i.e. "majority vote"). This automated image processing pipeline was successful for all subjects. Final ROIs were visually inspected by a board-certified neuroradiologist (JES). Cerebellar lobular volumes were subsequently estimated, resulting in 13 ROIs for each hemisphere (Figure 1). MAGeT-derived cerebellar volumes have high agreement compared to gold-standard manual tracings (total k =0.93, individual lobule k=0.73) (42).

Statistical Analyses:

Data was then imported into the R statistical environment (44). Volumetric measurements were first visually inspected and assessed for normality via histograms and quantile-quantile plots. ROI measurements approximated normality for all ROIs, although there were a few outliers for smaller ROIs (e.g. lobule I/II). ROIs were also aggregated to obtain derived estimates of cerebellar lobar volumes (anterior lobe, **AL**: lobules I-V; superior posterior lobe, **SPL**: lobules VI, Crus I-II, lobule VIIB; inferior posterior lobe, **IPL**: lobules VIIIA,

VIIIB, IX), based on definitions outlined by Mankiw et al. (43). Total cerebellum was calculated as the sum of all ROIs for both hemispheres.

Group differences in cerebellar volumes were visualized graphically and subsequently assessed statistically using ANOVA after adjusting for age, sex, and race. *Relative* group differences were also assessed by repeating the analysis and including total brain volume (TBV) as an additional covariate. Effect sizes for lobar and lobular ROI group differences were estimated by calculating Cohen's d (45). Group differences in absolute and relative lobular cerebellar volumes were assessed with MANCOVA, also including age, sex, and race as covariates. Because it is considered robust to potential violations of the assumptions of MANOVA, we used the Pillai trace as the test statistic (46). Specific lobule-level group differences were further assessed with *post-hoc* ANOVA corrected for multiple testing with the False Discovery Rate (FDR) (47).

Multivariate Relationships:

High collinearity was observed among cerebellar ROIs. Therefore, a series of additional analyses were performed to characterize inter-cerebellar relationships. Because different multivariate methods each carry their own strengths, biases, and limitations, we applied several different approaches. First, lobule-level cerebellar correlations were compared between groups via the Mantel test, a common global test of the element-by-element correlations between two matrices of equal dimensions (48). Statistical significance was obtained via permutation, using 5000 replicates to estimate the null. This test is constrained to linear effects, and does not provide insight on why two matrices are similar. Therefore, hierarchical clustering using Euclidean distances was then applied to each group separately, after adjusting for TBV and demographic covariates (49). As an alternative method of data reduction, multigroup principal component analysis (PCA) was subsequently performed on demographic and TBV-residualized data. The optimal number of components was determined via scree plot; a three-component solution explained 60% of the total variance in the TD group and 65% of the variance in 22q11DS. Common factor loadings from multigroup PCA were calculated (50, 51); this method is conceptually similar to traditional PCA, but accounts for known group structure in the data.

Prior studies have found aberrant structural connectivity in the supratentorial brain of subjects with 22q11DS (11, 30, 31). In order to investigate inter-cerebellar connectivity, undirected binary structural connectivity graphs (52) were then constructed using the *iGraph* and *BrainGraph* packages in R (53–55) for 22q11DS and TD groups separately. Given that the density of a network can influence many network statistics (56), the network properties were calculated using a range of graph connection density thresholds ranging from 10% to 40%. Several common graph-level network statistics (clustering coefficient, characteristic path length, global transitivity, Louvain modularity, and degree assortativity) were calculated across all network densities (11, 55). Three brain-specific measures were assessed, namely lobar assortativity (number of interlobar connections versus intra-lobar connections), lobe-hemisphere assortativity (similar to lobar assortativity, but with each lobe hemisphere considered a different region), and hemispheric asymmetry index (the difference in the number of left and right intra-hemispheric connections relative to the average connections of

both hemisphere, conceptually similar to laterality index) (55). Group differences in network statistics were assessed by calculating a standardized difference score (TD–22q11DS) for each statistic and graph density, and comparing to null distributions via permutation with 5000 replicates each.

Cerebro-Cerebellar Connectivity:

In order to examine how cerebellar morphology relates to the more well-established 22q11DS supratentorial endophenotype, MAGeT-derived lobar ROIs were compared to vertex-level measures of cerebral cortical thickness (CT) obtained via the CIVET pipeline(57). In order to calculate CT, differences in gray and white matter surfaces were fitted using deformable surface-mesh models and nonlinearly aligned toward a template surface (58–60). The gray and white matter surfaces were resampled into native space. CT was measured in native-space using the linked distance between the white and pial surfaces (59, 61). Linear regression models were then used to assess cerebellar ROI x diagnosis interactions on vertex-level measures of CT, after adjusting for age, sex, race, TBV, and main effects. Multiple testing was controlled using FDR (47).

Brain-Behavior Relationships:

Finally, exploratory brain-behavior analyses were performed, examining within-group associations between DSM axis I psychiatric disorders and relative cerebellar volumes in 22q11DS. Because the sample was underpowered, cerebellar lobe volumes were combined (left + right, i.e. 3 ROIs total) to compare with four clinically-assessed aggregate categories of psychiatric disease (psychosis, anxiety, attention, and major depression). Participants were considered part of the psychosis group if an individual had been diagnosed with schizophrenia, schizoaffective disorder, or psychosis not otherwise specified. Cohen's d based on diagnoses were calculated for each lobe. As an alternative exploratory method, we also constructed a continuous measure of psychosis (root-transformed SIPS sum score) for all 22q11DS subjects, and compared this measure to cerebellar lobule volumes via multiple regression. In addition to including cerebellar lobules as predictors, our demographic variables and TBV were also included as covariates in this analysis.

Results:

Total brain volumes in 22q11DS were lower by 11.3% relative to TD controls (999.5cm^3 versus 1126.6cm^3). On average, cerebellar volumes were 17.3% smaller in the 22q11DS group (115.8cm^3 versus 137.2cm^3), a statistically significant difference (F^1_{144}=101.35, p-value < 0.0001). There was a strong correlation between total brain and total cerebellar volumes (r=0.74, p-value< 0.0001). Nevertheless, group differences in relative cerebellar volume remained statistically significant even after adjusting for TBV (F^1_{143}=51.0, p-value<0.0001). Figure 2 summarizes these findings.

Table 2 and Figure 3 summarize group differences in cerebellar lobar and lobular volumes. Absolute cerebellar lobular volumes in the 22q11DS group were significantly different compared to TD controls (Pillai=0.6215, p-value<0.0001). *Post-hoc* ANOVA found significantly smaller volumes for all cerebellar ROIs (FDR-corrected p-values all <0.0001).

Regions of interest in the posterior lobes generally had larger group differences relative to the anterior lobe. Areas with the largest differences included Crus I, Crus II, lobule VIIB, lobule VIIIA, and cerebellar white matter. After adjusting for total brain volumes, relative cerebellar volumes remained significantly reduced in 22q11DS (Pillai=0.7169, p-value<0.0001), with all *post-hoc* FDR- corrected p-values <0.0002.

Figure S1 summaries the intra-regional relationships among cerebellar ROIs. Global correlational patterns were similar between TD and 22q11DS groups (Mantel test p-value = 0.0002). The strongest correlations were observed between contralateral homologues (e.g. left and right lobule V) and with other measures in the same cerebellar lobe (e.g. anterior lobe). Similarly, hierarchical clustering (Figure S1B) showed tight coupling between contralateral homologues, and generally replicated cerebellar lobar anatomy in both groups. Lobar-specific clustering was somewhat less pronounced in 22q11DS relative to controls. PCA suggested that three factors explained the majority of the variance for all 26 cerebellar ROIs (Figure S1C). Multigroup PCA found >96% similarity in TD, 22q11DS, and common (TD + 22q11DS) factor loadings for all components; we therefore only report common loadings. The dominant component (PC1) explained over a third of the variance and loaded on all ROIs similarly, i.e. a “global cerebellar” factor. PC2 identified a superior-inferior gradient in the cerebellum, with relatively symmetric loadings on contralateral homologues. PC3 identified associations between the flocculonodular lobe (lobule X) with lobules IV, V, and VIIIB, again with highly symmetric factor loadings.

Graph-level network statistics of the structural connectivity of the cerebellum are provided in Figure 4. Based on common graph-level statistics, the connectivity of the cerebellum was similar between groups. The TD group had somewhat higher modularity (a measure of community structure in networks), over all network densities (62). Lobe assortativity (a preference for nodes to assort by cerebellar lobe), also was higher in the TD group. Permutation tests found that for most measures (Figure 4C), group differences were not statistically significant. The exception was for lobe and lobe-hemisphere assortativity, which were significantly higher in the TD group over most network densities.

Cerebro-cerebellar interactions are provided in Figure 5. Significant total cerebellum x group interactions were most pronounced in the bilateral frontal cortex, cingulate cortex, and occipitotemporal cortex. For both AL and IPL seeds, only a few vertices reached statistical significance, and these tended to be in inferior occipitotemporal and orbitofrontal regions. In contrast, there were substantially more widespread, statistically significant SPL x group interactions that involved large regions of the right greater than left frontal lobe, temporal lobe, and bilateral cingulate cortex. These areas were associated with negative beta weights, indicative of disproportionately thicker cortex in the 22q11DS group with increasing SPL volume relative to TD controls. Post-hoc analyses demonstrated that the effects in SPL were primarily being driven by cerebro-cerebellar relationships involving Crus I, and to a lesser extent lobule VI (Figure S2).

Figure S3 summarizes relationships between cerebellar lobar volumes and categories of psychiatric disease in 22q11DS. Exploratory brain-behavioral analyses found a statistical trend towards different lobar cerebellar volumes in individuals with psychosis relative to

the subgroup without psychosis (Pillai=0.1007, p-value=0.0526). Post hoc tests suggested that the anterior lobe was relatively larger in individuals with a psychotic disorder (uncorrected p-value= 0.0129, corrected p-value=0.038), and that the superior posterior lobe was relatively smaller (uncorrected p-value=0.0530, corrected p-value=0.1078). Although the estimated effect sizes for psychosis were reasonably large (Cohen's d=0.81 and −0.77, respectively), the precision of these estimates was limited by the small sample size of the psychotic subgroup (n=9). Lobar associations with other psychiatric disease categories (e.g. depression) were not statistically significant. In contrast, multiple regression found that when predicting SIPS sum score in 22q11DS subjects, a model including cerebellar lobules as predictors had a significantly better fit than one that only included demographic variables and TBV (df=13, p-value = 0.0126); this association was largely driven by the predictive power of Crus I volumes (FDR corrected p-value=0.0136). Table S3 and Figures S4 and S5 summarize these findings.

Discussion:

While traditionally considered a motor structure, the cerebellum is increasingly recognized as having a role in cognition, affect, and the development of neuropsychiatric disorders (22, 23, 63, 64). For example, individuals with cerebellar atrophy (e.g. olivo-ponto-cerebellar atrophy) demonstrate deficits in language, executive function, and visuospatial abilities (65). The cerebellum demonstrates an extraordinarily complex functional topography based on regional differences in cerebrocerebellar connectivity, with the vast majority of connections made to association areas (32, 66, 67). Both connectivity and lesion studies suggest that the motor functions traditionally ascribed to the cerebellum are largely confined to the anterior lobe (68). In contrast, fibers from the posterior lobe preferentially connect to parietal and premotor cortex (69) and are correlated with measures of cognition, affect, and emotion (65, 67, 70, 71).

The current study provides the first comprehensive, systematic analysis of cerebellar volumetry in 22q11DS at multiple levels of spatial resolution. We found statistically significant and near-universally decreased cerebellar volumes in 22q11DS at global, lobar, and lobular scales, with some evidence that posterior lobules are disproportionately influenced. Our global cerebellar findings are concordant with prior neuroimaging studies that have similarly reported smaller cerebellar volumes in 22q11DS (9, 20, 72–78). For example, a meta-analysis on 141 subjects with 22q11DS found substantially smaller mean global cerebellar volumes compared to 106 TD controls (Hedges' $g = -1.25 \pm 95\%$ CI [−1.56, −0.95]) (79); this effect size is comparable to a similar calculation based on current study data (Hedges' $g = -1.69 \pm 95\%$ CI [−2.07, −1.31]).

Many of our lobule-level cerebellar ROIs had moderate ($0.8<|d|>0.5$) or large ($|d|>0.8$) TBV-adjusted group differences, with mean |d| of 0.64 and a range of −0.96 – −0.29. Group effects for many regions were comparable to the most impacted ICV-adjusted subcortical ROIs in 22q11DS, for example as estimated by the ENIGMA-22 consortium (e.g. hippocampus d ~ −0.90, lateral ventricle d ~ 0.90) (80). Group differences in cerebellar volume were also comparable to those cortical thickness ROIs with the strongest effects of the 22q11DS deletion, which have estimates ranging up to 0.87 (mean |d| = 0.39,

range −0.59 – 0.87) (12). The group effects we observe in the cerebellum were somewhat smaller in magnitude compared to those observed for the most impacted ICV-adjusted cortical surface area ROIs (mean |d| = 0.56, range −1.53 – 0.50) (12). Nevertheless when these findings are considered in aggregate, the cerebellum ranks among the most impacted neuroanatomic regions in 22q11DS, paralleling observations from the Df16A$^{+/-}$ mouse model of 22q11DS (81).

Despite regional differences in cerebellar volumes in 22q11DS, we observed that patterns of inter-cerebellar relationships were generally similar between 22q11DS and TD groups regardless of multivariate approach. Our observations of 1) a dominant global factor influencing all cerebellar ROIs and 2) strong inter-hemispheric correlations between homologous regions are both properties that have been described for numerous cerebral and subcortical ROIs; there is evidence that these patterns are largely genetically-mediated (82–84). PCA also identified a strong gradient along the superior-inferior cerebellar axis, paralleling the principal functional neuroanatomy of the cerebellum (63). The third principal component involved the larger ROIs of the anterior lobe, flocculonodular lobe, and lobule VIII, all regions associated with motor functions (85). These findings suggest that much of the variance in cerebellar volume can be explained by a few shared global factors influencing multiple ROIs simultaneously.

Although patterns of cerebello-cerebellar connectivity were similar between groups, our graph theoretical analyses did identify evidence of reduced network cohesion in 22q11DS relative to TD controls, as evidenced by reduced modularity, lobe assortativity, and lobe-hemisphere assortativity. Assortativity is a measure of the resilience of a network due to interconnected hubs, while modularity is a measure of the strength of the community structure in a network (62, 86). We have previously reported disrupted structural connectivity in the cerebrum in 22q11DS (11); disrupted structural connectivity in the supratentorial brain has also been associated with the emergence of psychosis in 22q11DS (30, 31). Although there are no prior studies on cerebellar dysconnectivity in 22q11DS, decreased cerebello-cerebellar connectivity has been reported in schizophrenia (87).

We found aberrant cerebro-cerebellar associations in 22q11DS, primarily with the SPL, and with *post hoc* analysis suggesting these findings were largely driven by Crus I and lobule VI. To our knowledge, this is the first study to examine these relationships directly. Prior work has shown that there are widespread anomalies in CT in 22q11DS (12, 15, 19, 88). CT is generally *thicker* in 22q11DS relative to TD controls, with widespread differences in the bilateral frontal lobes and parasagittal medial cerebrum. In contrast, both superior temporal gyrus and cingulate cortex are significantly *thinner* in 22q11DS. We found significant SPL x group interactions associated with all of these cortical regions. These analyses provide evidence that our novel cerebellar findings are probably related to the more well-established morphological differences that have been observed in the supratentorial brain in 22q11DS, although the causal relationships remain unknown.

There is growing evidence that both aberrant cerebellar structure and cerebro-cerebellar connectivity contribute to the pathophysiology of schizophrenia; clinical, cognitive, structural, and functional neuroimaging studies all point towards the cerebellum as a likely

contributor to the schizophrenia endophenotype (26, 89, 98, 90–97). For example, in a large meta-analysis, Moberget et al. found that the cerebellar gray matter was reduced in 983 subjects with schizophrenia compared to 1349 healthy controls, with a pooled Cohen's d=−0.35 (95). Regions of the cerebellum with strong fronto-parietal connectivity have particular volumetric reductions in schizophrenia, with effect sizes comparable to many regions of the brain with much more well-established associations with schizophrenia, e.g. the hippocampus (95). Although there are no prior studies examining the associations between cerebellar substructure and psychosis in 22q11DS specifically, Kates et al. reported that longitudinal decreases in total cerebellar volumes are predictive of prodromal psychosis in children and adolescents with 22q11DS (20).

Our within-group exploratory brain-behavior analysis found relatively weak evidence that that individuals with both 22q11DS and psychosis have disproportionately smaller superior posterior cerebellums. Prior studies have suggested that the superior posterior lobules VI, Crus I, and Crus II are particularly associated with psychosis in non-deleted populations (99, 100). Thus, disproportionate volume loss in the posterior cerebellum may increase liability to psychosis in 22q11DS via a similar mechanism. Although it is tempting to hypothesize that cerebellar anomalies along an anterior-posterior gradient may be related to psychopathology in 22q11DS, it is noteworthy that SPL volumes also dominate the lateral cerebellum (e.g. Figure 3), and neurodevelopmental anomalies along the medial-lateral axis are also possible (32). These findings warrant further investigation.

Limitations:

There are important limitations that must be considered when interpreting our findings. First, our sample was limited to relatively higher-functioning subjects; this decision was made to ensure high-quality neurocognitive, clinical, and neuroimaging data. However, this likely underestimates the morphological group differences in 22q11DS, and also likely reduces the prevalence of psychosis in our sample. Second, although the TD and 22q11DS groups were matched demographically, the 22q11DS group remained significantly older. Age effects were therefore partially controlled statistically in our analysis. Repeat analyses with more comparable age ranges produced similar results, which is reassuring. Finally, results from our exploratory brain-behavior analyses should be interpreted with caution, in part because our psychosis^{+} group is confounded with the use of antipsychotic medications. Our findings were also statistically weak and driven by a relatively small number of subjects with a clinical diagnosis of a psychotic disorder, although we did identify more robust associations when treating psychosis as a continuous variable. Nevertheless, further research on larger samples will be critical in order to better characterize the effect of aberrant cerebellar morphology on the 22q11DS neuropsychiatric phenotype.

Supplementary Material

Refer to Web version on PubMed Central for supplementary material.

Acknowledgements:

This study was supported by NIH grants MH087626, MH087636MH089983, and a grant from the Stanford MCHRI Uytengsu-Hamilton 22q11 Neuropsychiatry Research Awards Program. The Philadelphia Neurodevelopmental Cohort was supported by NIH grants MH089983 and MH089924. DRR: R01 MH119185;R01 MH120174; R56 AG066656. We would also like to thank the children and families of the “22q and You” center of the Children’s Hospital of Philadelphia.

References:

1. Sullivan PF, Kendler KS, Neale MC (2014): Schizophrenia as a Complex Trait. Arch Gen Psychiatry. 60: 1187–1192.
2. International Schizophrenia Consortium (2008): Rare chromosomal deletions and duplications increase risk of schizophrenia. Nature. 455: 237–41. [PubMed: 18668038]
3. Working Group of the Psychiatric Genomics Consortium S (2015): Biological Insights From 108 Schizophrenia-Associated Genetic Loci. Nature. 511: 421–427.
4. Ripke S, O’Dushlaine C, Chambert K, Moran JL, Kähler AK, Akterin S, et al. (2013): Genome-wide association analysis identifies 13 new risk loci for schizophrenia. Nat Genet. 45: 1150–9. [PubMed: 23974872]
5. Murphy KC, Jones LA, Owen MJ (1999): High rates of schizophrenia in adults with velo- cardio-facial syndrome. Arch Gen Psychiatry. 56: 940–5. [PubMed: 10530637]
6. Bassett A, Chow E (1999): 22Q11 Deletion Syndrome: a Genetic Subtype of Schizophrenia. Biol Psychiatry. 46: 882–91. [PubMed: 10509171]
7. Liu H, Abecasis GR, Heath SC, Knowles A, Demars S, Chen Y-J, et al. (2002): Genetic variation in the 22q11 locus and susceptibility to schizophrenia. Proc Natl Acad Sci U S A. 99: 16859–16864. [PubMed: 12477929]
8. Mcdonald-Mcginn DM, Sullivan K, Marino B, Swillen A, Vortsman J, Zackai E, et al. (2015): 22q11.2 Deletion Syndrome. Nat Rev Dis Prim. 1: 621–626.
9. Eliez S, Schmitt JE, White CD, Reiss AL (2000): Children and Adolescents With Velocardiofacial Syndrome: A Volumetric MRI Study. Am J Psychiatry. 157: 409–415. [PubMed: 10698817]
10. Schmitt JE, Yi J, Roalf D, Loevner L, Ruparel K, Whinna D, et al. (2014): Incidental radiologic findings in the 22q11.2 deletion syndrome. AJNR Am J Neuroradiol. 35: 2186–91. [PubMed: 24948496]
11. Schmitt JE, Yi J, Calkins ME, Ruparel K, Roalf DR, Cassidy A, et al. (2016): Disrupted anatomic networks in the 22q11.2 deletion syndrome. NeuroImage Clin. 12: 420–428. [PubMed: 27622139]
12. Sun D, Ching CRK, Lin A, Forsyth JK, Kushan L, Vajdi A, et al. (2018): Large-scale mapping of cortical alterations in 22q11.2 deletion syndrome: Convergence with idiopathic psychosis and effects of deletion size. Mol Psychiatry. 25: 1822–1834. [PubMed: 29895892]
13. Villalon-Reina JE, Martínez K, Qu X, Ching CRK, Nir T, Kothapalli D, et al. (2019): Altered White Matter Microstructure in 22q11.2 Deletion Syndrome: A Multi-Site Tensor Imaging Study. Mol Psychiatry. 25: 2818–2831. [PubMed: 31358905]
14. Tan GM, Arnone D, McIntosh AM, Ebmeier KP (2009): Meta-analysis of magnetic resonance imaging studies in chromosome 22q11.2 deletion syndrome (velocardiofacial syndrome). Schizophr Res. 115: 173–81. [PubMed: 19819113]
15. Jalbrzikowski M, Jonas R, Senturk D, Patel A, Chow C, Green MF, Bearden CE (2013): Structural abnormalities in cortical volume, thickness, and surface area in 22q11.2 microdeletion syndrome: Relationship with psychotic symptoms. NeuroImage Clin. 3: 405–15. [PubMed: 24273724]
16. Schmitt JE, Vandekar S, Yi J, Calkins ME, Ruparel K, Roalf DR, et al. (2015): Aberrant Cortical Morphometry in the 22q11.2 Deletion Syndrome. Biol Psychiatry. 78: 135–143. [PubMed: 25555483]
17. Scariati E, Padula MC, Schaer M, Eliez S (2016): Long-range dysconnectivity in frontal and midline structures is associated to psychosis in 22q11.2 deletion syndrome. J Neural Transm. 123: 823–839. [PubMed: 27094177]

18. Debbané M, Lazouret M, Lagioia A, Schneider M, Van De Ville D, Eliez S (2012): Resting-state networks in adolescents with 22q11.2 deletion syndrome: associations with prodromal symptoms and executive functions. Schizophr Res. 139: 33–9. [PubMed: 22704643]
19. Bearden CE, van Erp TGM, Dutton R a, Tran H, Zimmermann L, Sun D, et al. (2007): Mapping cortical thickness in children with 22q11.2 deletions. Cereb Cortex. 17: 1889–98. [PubMed: 17056649]
20. Kates WR, Antshel KM, Faraone SV., Fremont WP, Higgins AM, Shprintzen RJ, et al. (2011): Neuroanatomic predictors to prodromal psychosis in velocardiofacial syndrome (22q11.2 deletion syndrome): A longitudinal study. Biol Psychiatry. 69: 945–952. [PubMed: 21195387]
21. Eliez S, Blasey CM, Schmitt JE, White CD, Hu D, Reiss AL (2001): Velocardiofacial Syndrome : Are Structural Changes in the Temporal and Mesial Temporal Regions Related to Schizophrenia? Am J Psychiatry. 158: 447–453. [PubMed: 11229987]
22. Schmahmann JD, Guell X, Stoodley CJ, Halko MA (2019): The Theory and Neuroscience of Cerebellar Cognition. Annu Rev Neurosci. 42: 337–364. [PubMed: 30939101]
23. Schmahmann JD (2000): The role of the cerebellum in affect and psychosis. J Neurolinguistics. 13: 189–214.
24. Seidter RD, Purushotham A, Kim SG, Uğurbil K, Willingham D, Ashe J (2002): Cerebellum activation associated with performance change but not motor learning. Science. 296: 2043–2046. [PubMed: 12065841]
25. Kim SG, Uğurbil K, Strick PL (1994): Activation of a cerebellar output nucleus during cognitive processing. Science. 265: 949–951. [PubMed: 8052851]
26. Andreasen NC, Pierson R (2008): The Role of the Cerebellum in Schizophrenia. Biol Psychiatry. 64: 81–88. [PubMed: 18395701]
27. Bruchhage MMK, Bucci MP, Becker EBE (2018): Cerebellar involvement in autism and ADHD. Handb Clin Neurol. 155: 61–72. [PubMed: 29891077]
28. Eliez S, Schmitt JE, White CD, Wellis VG, Reiss AL (2001): A quantitative MRI study of posterior fossa development in velocardiofacial syndrome. Biol Psychiatry. 49: 540–6. [PubMed: 11257239]
29. Bish JP, Pendyal A, Ding L, Ferrante H, Nguyen V, McDonald-McGinn D, et al. (2006): Specific cerebellar reductions in children with chromosome 22q11.2 deletion syndrome. Neurosci Lett. 399: 245–248. [PubMed: 16517069]
30. Sandini C, Scariati E, Padula MC, Schneider M, Schaer M, Van De Ville D, Eliez S (2018): Cortical Dysconnectivity Measured by Structural Covariance Is Associated With the Presence of Psychotic Symptoms in 22q11.2 Deletion Syndrome. Biol Psychiatry Cogn Neurosci Neuroimaging. 3: 433–442. [PubMed: 29735153]
31. Padula MC, Scariati E, Schaer M, Sandini C, Ottet MC, Schneider M, et al. (2017): Altered structural network architecture is predictive of the presence of psychotic symptoms in patients with 22q11.2 deletion syndrome. NeuroImage Clin. 16: 142–150. [PubMed: 28794975]
32. Buckner RL, Krienen FM, Castellanos A, Diaz JC, Thomas Yeo BT (2011): The organization of the human cerebellum estimated by intrinsic functional connectivity. J Neurophysiol. 106: 2322–2345. [PubMed: 21795627]
33. Jalali GR, Vorstman JAS, Errami A, Vijzelaar R, Biegel J, Shaikh T, Emanuel BS (2008): Detailed analysis of 22q11.2 with a high density MLPA probe set. Hum Mutat. 29: 433–40. [PubMed: 18033723]
34. Miller TJ, McGlashan TH, Rosen JL, Cadenhead K, Cannon T, Ventura J, et al. (2004): Prodromal assessment with the structured interview for prodromal syndromes and the scale of prodromal symptoms: Predictive validity, interrater reliability, and training to reliability. Schizophr Bull. 290: 703–715.
35. Kaufman J, Birmaher B, Brent D, Rao U, Flynn C, Moreci P, et al. (1997): Schedule for Affective Disorders and Schizophrenia for School-Age Children-Present and Lifetime Version (K-SADS-PL): initial reliability and validity data. J Am Acad Child Adolesc Psychiatry. 36: 980–8. [PubMed: 9204677]
36. First M, Gibbon M (2004): The Structured Clinical Interview for DSM-IV Axis I Disorders (SCID-I) and the Structured Clinical Interview for DSM-IV Axis II Disorders (SCID-II). In:

Hilsenroth M, Segal D, editors. Compr Handb Psychol assessment, Vol 2Personality Assessment. Hoboken, NJ: John Wiley & Sons, pp 134–143.

37. Tang S, Yi JJ, Calkins M, Whinna D, Kohler C, Souders M, et al. (2013): Psychiatric disorders in 22q11.2 deletion syndrome are prevalent but undertreated. Psychol Med. 44: 1267–1277. [PubMed: 24016317]
38. Satterthwaite TD, Elliott MA, Ruparel K, Loughead J, Prabhakaran K, Calkins ME, et al. (2013): Neuroimaging of the Philadelphia Neurodevelopmental Cohort. Neuroimage. 86: 544–53. [PubMed: 23921101]
39. Ad-Dab'bagh Y, Lyttelton O, Muehlboeck J, Lepage C, Einarson D, Mok K, et al. (2006): The CIVET image-processing environment: A fully automated comprehensive pipeline for anatomcal neuroimaging research. In: Corbetta M, editor. Proc 12th Annu Meet Organ Hum Brain Mapp. Florence, Italy.
40. Collins D, Neelin P, Peters T, Evans AC (1994): Automatic 3D intersubject registration of MR volumetric data in standardized Talairach space. J Comput Assist Tomogr. 18: 192–205. [PubMed: 8126267]
41. Sled JG, Zijdenbos AP, Evans AC (1998): A nonparametric method for automatic correction of intensity nonuniformity in MRI data. IEEE Trans Med Imaging. 17: 87–97. [PubMed: 9617910]
42. Park MTM, Pipitone J, Baer LH, Winterburn JL, Shah Y, Chavez S, et al. (2014): Derivation of high-resolution MRI atlases of the human cerebellum at 3T and segmentation using multiple automatically generated templates. Neuroimage. 95: 217–231. [PubMed: 24657354]
43. Mankiw C, Park MTM, Reardon PK, Fish AM, Clasen LS, Greenstein D, et al. (2017): Allometric analysis detects brain size-independent effects of sex and sex chromosome complement on human cerebellar organization. J Neurosci. 37: 5221–5231. [PubMed: 28314818]
44. R Core Team (2020): R: A language and environment for statistical computing. Vienna, Austria. Retrieved from http://www.r-project.org/.
45. Cohen J (1988): Statistical Power Analysis for the Behavioral Sciences. Lawrence Erlbaum Associates.
46. Pillai K (1955): Some new test criteria in multivariate analysis. Ann Math Stat. 26: 117–121.
47. Genovese CR, Lazar NA, Nichols T (2002): Thresholding of Statistical Maps in Functional Neuroimaging Using the False Discovery Rate. Neuroimage. 15: 870–878. [PubMed: 11906227]
48. Mantel N (1967): The Detection of Disease Clustering and a Generalized Regression Approach. Cancer Res. 214: 637–637.
49. Warnes G, Bolker B, Bonebakker L, Gentleman R, Huber W, Liaw A, et al. (2015): gplots: various R tools for plotting data.
50. Eslami A, Qannari EM, Kohler A, Bougeard S (2014): Multivariate analysis of multiblock and multigroup data. Chemom Intell Lab Syst. 133: 63–69.
51. Krzanowski JW (2018): Principal Component Analysis in the Presence of Group Structure. J R Stat Soc Ser C (Appl Stat). 33: 164–168.
52. Alexander-Bloch A, Giedd JN, Bullmore E (2013): Imaging structural co-variance between human brain regions. Nat Rev Neurosci. 14: 322–36. [PubMed: 23531697]
53. Csárdi G, Nepusz T (2015): igraph: network analysis and visualization. R Ref Man.
54. Csárdi G, Nepusz T (2006): The igraph software package for complex network research. InterJournal Complex Syst. 1695: 1695.
55. Watson CG, Stopp C, Newburger JW, Rivkin MJ (2018): Graph theory analysis of cortical thickness networks in adolescents with d-transposition of the great arteries. Brain Behav. 8: 1–15.
56. Bassett DS, Bullmore E, Verchinski BA, Mattay VS, Weinberger DR, Meyer-Lindenberg A (2008): Hierarchical organization of human cortical networks in health and schizophrenia. J Neurosci. 28: 9239–48. [PubMed: 18784304]
57. Lerch JP, Worsley K, Shaw WP, Greenstein DK, Lenroot RK, Giedd J, Evans AC (2006): Mapping anatomical correlations across cerebral cortex (MACACC) using cortical thickness from MRI. Neuroimage. 31: 993–1003. [PubMed: 16624590]

58. Kim JS, Singh V, Lee JK, Lerch J, Ad-Dab'bagh Y, MacDonald D, et al. (2005): Automated 3-D extraction and evaluation of the inner and outer cortical surfaces using a Laplacian map and partial volume effect classification. Neuroimage. 27: 210–21. [PubMed: 15896981]
59. MacDonald D, Kabani N, Avis D, Evans AC (2000): Automated 3-D extraction of inner and outer surfaces of cerebral cortex from MRI. Neuroimage. 12: 340–56. [PubMed: 10944416]
60. Robbins S, Evans AC, Collins DL, Whitesides S (2004): Tuning and comparing spatial normalization methods. Med Image Anal. 8: 311–23. [PubMed: 15450225]
61. Lerch J, Evans A (2005): Cortical thickness analysis examined through power analysis and a population simulation. Neuroimage. 24: 163–173. [PubMed: 15588607]
62. Newman MEJ (2006): Modularity and community structure in networks. Proc Natl Acad Sci U S A. 103: 8577–8582. [PubMed: 16723398]
63. Stoodley CJ, Schmahmann JD (2018): Functional topography of the human cerebellum, 1st ed. Handb Clin Neurol. (Vol. 154), Elsevier B.V.
64. Hoppenbrouwers SS, Schutter DJLG, Fitzgerald PB, Chen R, Daskalakis ZJ (2008): The role of the cerebellum in the pathophysiology and treatment of neuropsychiatric disorders: A review. Brain Res Rev. 59: 185–200. [PubMed: 18687358]
65. Tedesco AM, Chiricozzi FR, Clausi S, Lupo M, Molinari M, Leggio MG (2011): The cerebellar cognitive profile. Brain. 134: 3669–3683.
66. Krienen FM, Buckner RL (2009): Segregated fronto-cerebellar circuits revealed by intrinsic functional connectivity. Cereb Cortex. 19: 2485–2497. [PubMed: 19592571]
67. Strick PL, Dum RP, Fiez JA (2009): Cerebellum and nonmotor function. Annu Rev Neurosci. 32: 413–434. [PubMed: 19555291]
68. Palesi F, Tournier JD, Calamante F, Muhlert N, Castellazzi G, Chard D, et al. (2015): Contralateral cerebello-thalamo-cortical pathways with prominent involvement of associative areas in humans in vivo. Brain Struct Funct. 220: 3369–3384. [PubMed: 25134682]
69. Kelly RM, Strick PL (2003): Cerebellar loops with motor cortex and prefrontal cortex of a nonhuman primate. J Neurosci. 23: 8432–8444. [PubMed: 12968006]
70. Koppelmans V, Hoogendam YY, Hirsiger S, Mérillat S, Jäncke L, Seidler RD (2017): Regional cerebellar volumetric correlates of manual motor and cognitive function. Brain Struct Funct. 222: 1929–1944. [PubMed: 27699480]
71. Adamaszek M, D'Agata F, Ferrucci R, Habas C, Keulen S, Kirkby KC, et al. (2017): Consensus Paper: Cerebellum and Emotion. Cerebellum. 16: 552–576. [PubMed: 27485952]
72. Antshel KM, Abdulsabur N, Roizen N, Fremont W, Kates WR (2005): Sex differences in cognitive functioning in velocardiofacial syndrome (VCFS). Dev Neuropsychol. 28: 849–869. [PubMed: 16266252]
73. Gothelf D, Penniman L, Gu E, Eliez S, Reiss AL (2007): Developmental trajectories of brain structure in adolescents with 22q11.2 deletion syndrome: A longitudinal study. Schizophr Res. 96: 72–81. [PubMed: 17804201]
74. Campbell LE, Daly E, Toal F, Stevens A, Azuma R, Catani M, et al. (2006): Brain and behaviour in children with 22q11.2 deletion syndrome: a volumetric and voxel-based morphometry MRI study. Brain. 129: 1218–28. [PubMed: 16569671]
75. van Amelsvoort T, Daly E, Henry J, Robertson D, Ng V, Owen M, et al. (2004): Brain Anatomy in Adults With Velocardiofacial Syndrome With and WithoutSchizophrenia. Arch Gen Psychiatry. 61: 1085. [PubMed: 15520356]
76. Van Amelsvoort T, Daly E, Robertson D, Suckling J, Ng V, Critchley H, et al. (2001): Structural brain abnormalities associated with deletion at chromosome 22q11: Quantitative neuroimaging study of adults with velo-cardio-facial syndrome. Br J Psychiatry. 178: 412–419. [PubMed: 11331556]
77. Mitnick RJ, Bello JA, Shprintzen RJ (1994): Brain anomalies in velo-cardio-facial syndrome. Am J Med Genet. 54: 100–6. [PubMed: 8074159]
78. Haenssler AE, Baylis A, Perry JL, Kollara L, Fang X, Kirschner R (2020): Impact of Cranial Base Abnormalities on Cerebellar Volume and the Velopharynx in 22q11.2 Deletion Syndrome. Cleft Palate-Craniofacial J. 57: 412–419.

79. Rogdaki M, Gudbrandsen M, McCutcheon RA, Blackmore CE, Brugger S, Ecker C, et al. (2020): Magnitude and heterogeneity of brain structural abnormalities in 22q11.2 deletion syndrome: a meta-analysis. Mol Psychiatry. 25: 1704–1717. [PubMed: 31925327]
80. Ching CRK, Gutman BA, Sun D, Reina JV, Ragothaman A, Isaev D, et al. (2020): Mapping subcortical brain alterations in 22q11.2 deletion syndrome: Effects of deletion size and convergence with idiopathic neuropsychiatric illness. Am J Psychiatry. 177: 589–600. [PubMed: 32046535]
81. Ellegood J, Markx S, Lerch JP, Steadman PE, Genç C, Provenzano F, et al. (2014): Neuroanatomical phenotypes in a mouse model of the 22q11.2 microdeletion. Mol Psychiatry. 19: 99–107. [PubMed: 23999526]
82. Schmitt JE, Lenroot RK, Wallace GL, Ordaz S, Taylor KN, Kabani N, et al. (2008): Identification of genetically mediated cortical networks: a multivariate study of pediatric twins and siblings. Cereb cortex. 18: 1737–47. [PubMed: 18234689]
83. Schmitt JE, Lenroot RK, Ordaz SE, Wallace GL, Lerch JP, Evans AC, et al. (2009): Variance decomposition of MRI-based covariance maps using genetically informative samples and structural equation modeling. NeuroImage. 47: 56–64. [PubMed: 18672072]
84. Schmitt JE, Wallace GL, Rosenthal MA, Molloy EA, Ordaz S, Lenroot R, et al. (2007): A multivariate analysis of neuroanatomic relationships in a genetically informative pediatric sample. Neuroimage. 35: 70–82. [PubMed: 17208460]
85. Guell X, Schmahmann J (2020): Cerebellar Functional Anatomy: a Didactic Summary Based on Human fMRI Evidence. Cerebellum. 19: 1–5. [PubMed: 31707620]
86. Rubinov M, Sporns O (2010): Complex network measures of brain connectivity: uses and interpretations. NeuroImage. 52: 1059–69. [PubMed: 19819337]
87. Kim DJ, Kent JS, Bolbecker AR, Sporns O, Cheng H, Newman SD, et al. (2014): Disrupted modular architecture of cerebellum in schizophrenia: A graph theoretic analysis. Schizophr Bull. 40: 1216–1226. [PubMed: 24782561]
88. Schmitt JE, Vandekar S, Yi J, Calkins M, Ruparel K, Roalf D, et al. (2014): Aberrant Cortical Morphometry in the 22q11.2 Deletion Syndrome. Biol Psychiatry. 78: 135–143. [PubMed: 25555483]
89. Haijma S V, Van Haren N, Cahn W, Koolschijn PCMP, Hulshoff Pol HE, Kahn RS (2013): Brain volumes in schizophrenia: A meta-analysis in over 18 000 subjects. Schizophr Bull. 39: 1129–1138. [PubMed: 23042112]
90. Gupta CN, Calhoun VD, Rachakonda S, Chen J, Patel V, Liu J, et al. (2015): Patterns of gray matter abnormalities in schizophrenia based on an international mega-analysis. Schizophr Bull. 41: 1133–1142. [PubMed: 25548384]
91. Keller A, Castellanos FX, Vaituzis AC, Jeffries NO, Giedd JN, Rapoport JL (2003): Progressive loss of cerebellar volume in childhood-onset schizophrenia. Am J Psychiatry. 160: 128–133. [PubMed: 12505811]
92. Picard H, Amado I, Mouchet-Mages S, Olié JP, Krebs MO (2008): The role of the cerebellum in schizophrenia: An update of clinical, cognitive, and functional evidences. Schizophr Bull. 34: 155–172. [PubMed: 17562694]
93. Bottmer C, Bachmann S, Pantel J, Essig M, Amann M, Schad LR, et al. (2005): Reduced cerebellar volume and neurological soft signs in first-episode schizophrenia. Psychiatry Res - Neuroimaging. 140: 239–250.
94. Shinn AK, Baker JT, Lewandowski KE, Öngür D, Cohen BM (2015): Aberrant cerebellar connectivity in motor and association networks in schizophrenia. Front Hum Neurosci. 9: 1–16. [PubMed: 25653611]
95. Moberget T, Doan NT, Alnæs D, Kaufmann T, Córdova-Palomera A, Lagerberg TV., et al. (2018): Cerebellar volume and cerebellocerebral structural covariance in schizophrenia: A multisite mega-analysis of 983 patients and 1349 healthy controls. Mol Psychiatry. 23: 1512–1520. [PubMed: 28507318]
96. Collin G, HulshoffPol HE, Haijma SV., Cahn W, Kahn RS, van den Heuvel MP (2011): Impaired cerebellar functional connectivity in schizophrenia patients and their healthy siblings. Front Psychiatry. 2: 1–12. [PubMed: 21556272]

97. Daskalakis ZJ, Christensen BK, Fitzgerald PB, Fountain SI, Chen R (2005): Reduced cerebellar inhibition in schizophrenia: A preliminary study. Am J Psychiatry. 162: 1203–1205. [PubMed: 15930071]

98. Kim SE, Jung S, Sung G, Bang M, Lee SH (2021): Impaired cerebro-cerebellar white matter connectivity and its associations with cognitive function in patients with schizophrenia. npj Schizophr. 7. Available online.

99. Kühn S, Romanowski A, Schubert F, Gallinat J (2012): Reduction of cerebellar grey matter in Crus i and II in schizophrenia. Brain Struct Funct. 217: 523–529. [PubMed: 22131119]

100. He H, Luo C, Luo Y, Duan M, Yi Q, Biswal BB, Yao D (2019): Reduction in gray matter of cerebellum in schizophrenia and its influence on static and dynamic connectivity. Hum Brain Mapp. 40: 517–528. [PubMed: 30240503]

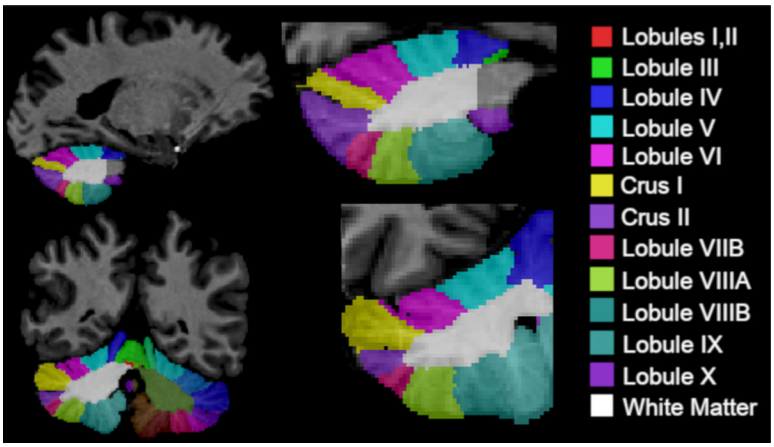

Figure 1:
Examples of MAGeT parcellations for lobule-level cerebellar regions of interest in four representative subjects with 22q11DS. Left and right cerebellar hemispheres are measured separately (legend is for left hemisphere ROIs only, labeled in a counter-clockwise order).

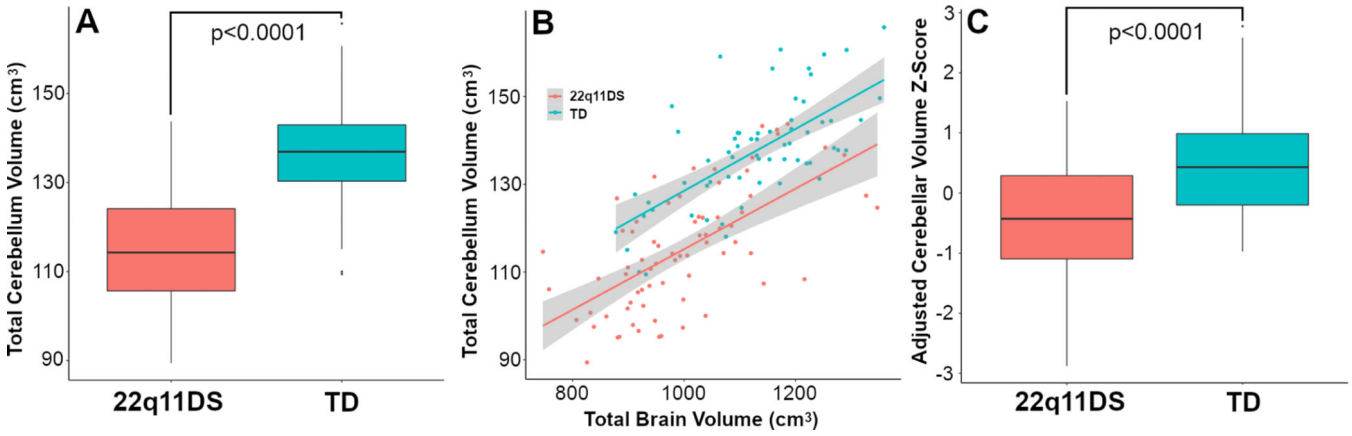

Figure 2:

Decreased cerebellar volumes in 22q11DS. Panel **A** reports raw volumetric group differences in total cerebellar volumes between subjects with 22q11DS and a TD control group. Panel **B** is a scatterplot demonstrating the correlation between total brain volume and total cerebellar volumes. Panel **C** also quantifies group differences, but after adjusting for age, sex, race, and total brain volumes.

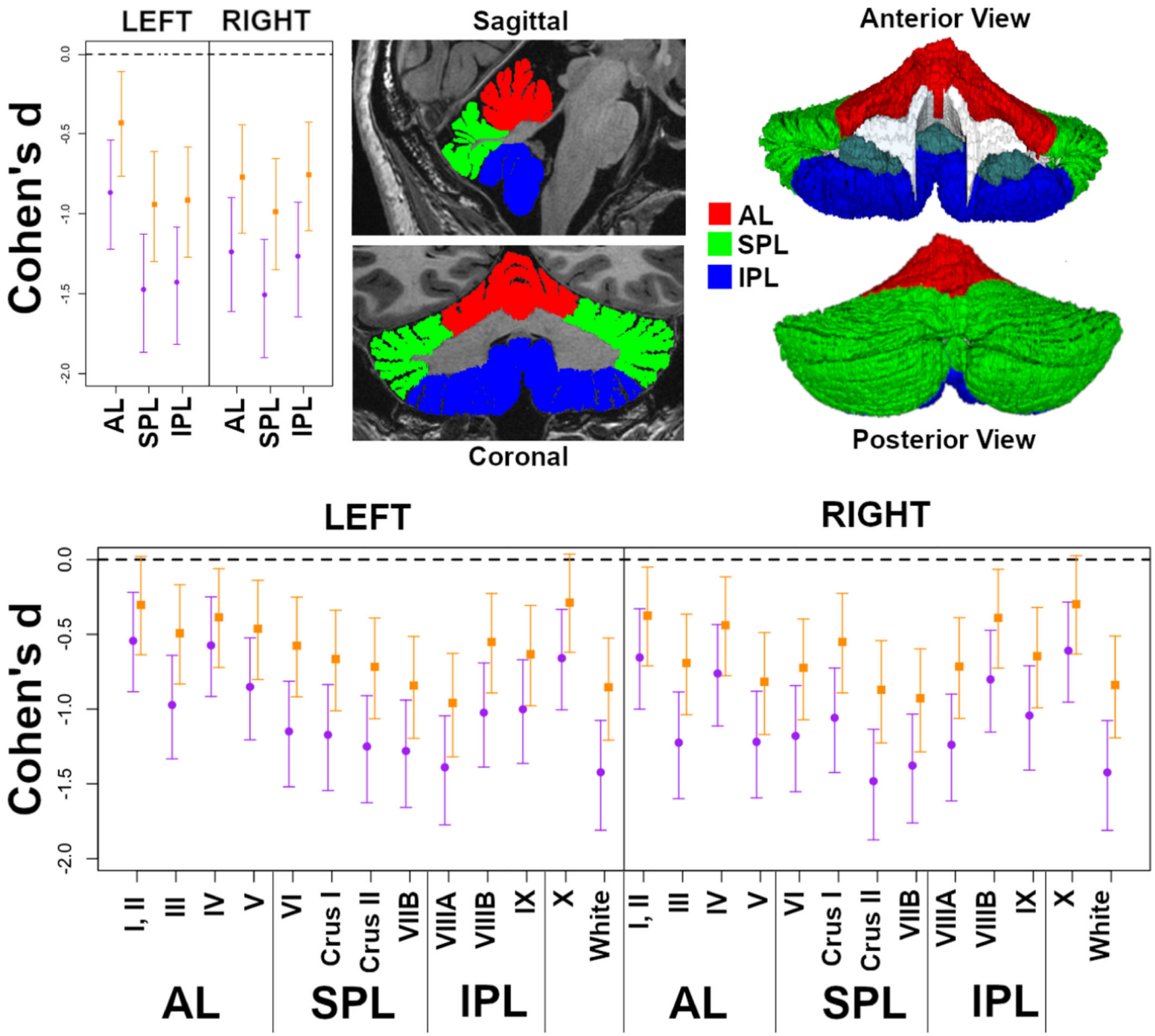

Figure 3:

Effect sizes (Cohen's d) for group differences in cerebellar lobes and lobules. Negative values indicate that TD volumes are greater than 22q11DS. Cohen's d without adjustment for TBV (purple circles) are shown, as well as TBV-adjusted values (orange squares). Error bars represent 95% confidence intervals. Lobar ROI definitions are shown both on cross-sectional images (top center) and a 3D surface (top right). Lobular-level ROI parcellations were provided in Figure 1.

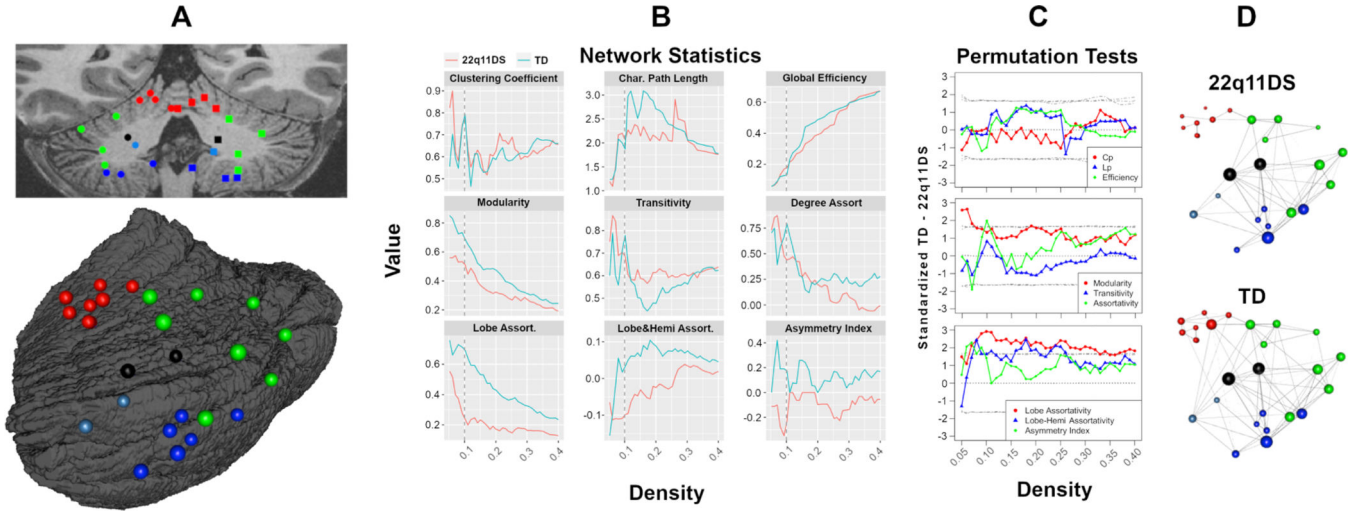

Figure 4:

Results from graph theoretical models. At left (Panel **A**), the centroid for each ROI is projected on a coronal slice, as well as a left posterior lateral oblique surface projection; each node is color coded based on lobe. At center (**B**), global network statistics for a range of graph densities are plotted for each group separately. Panel **C** displays results of permutation tests, with standardized TD - 22q11DS difference scores at each graph density; these plots are overlaid on null distributions, with gray lines indicating 5th, 50th, and 95th quantiles. Finally, panel **D** provides representative structural covariance graphs (density = 0.1) for each group.

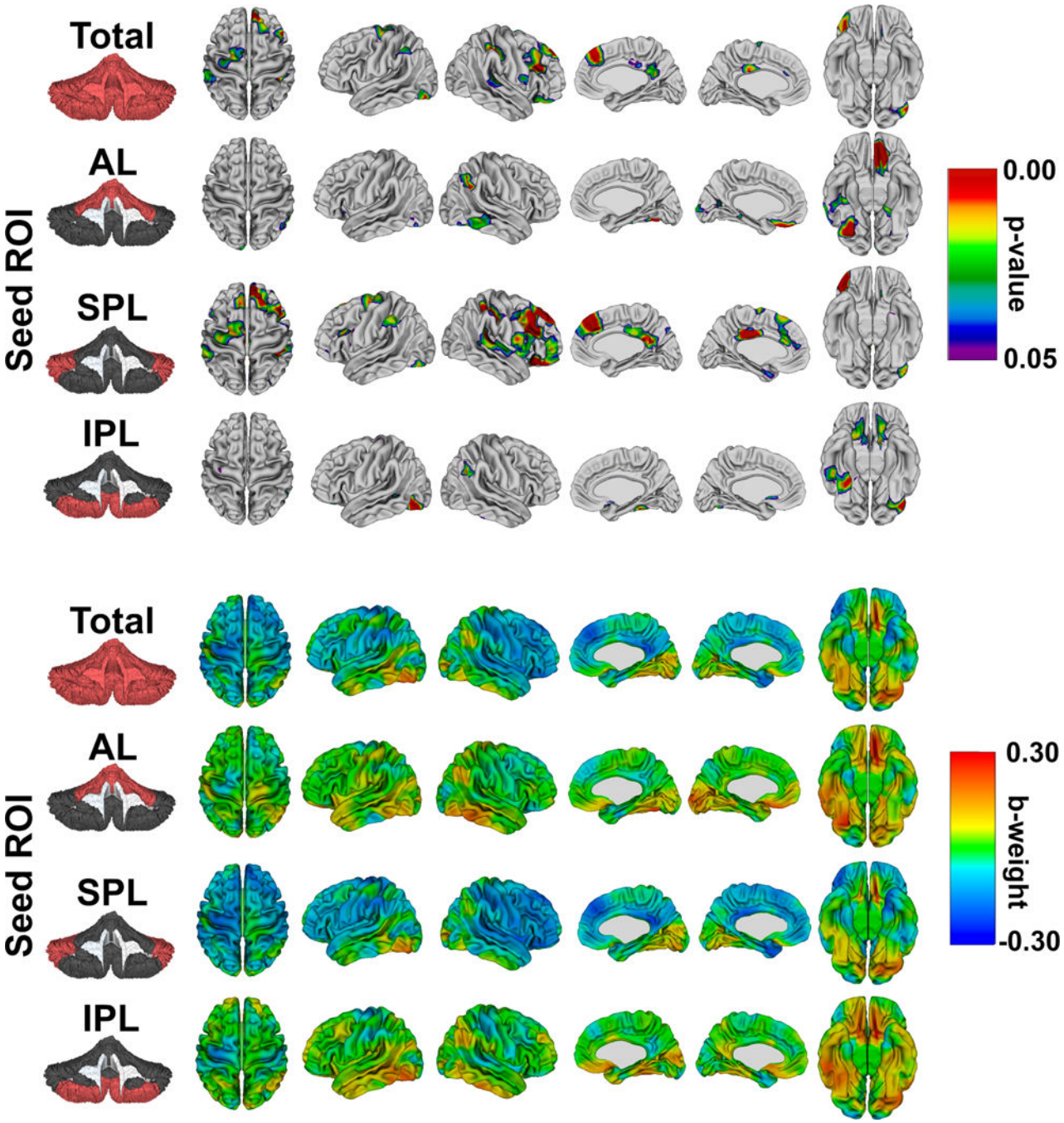

Figure 5:

Group differences in cerebro-cerebellar associations for cerebellar lobes. FDR-corrected probability maps (top) show statistically significant total and lobar cerebellum x group interactions on vertex-level measures of cortical thickness. The color maps (bottom) display the standardized b-weights for the ROI x diagnosis interaction (TD dummy coded 1, 22q11DS 0). Red indicates thicker cortex in the TD group with increasing volumes (relative to 22q11DS), with areas in blue having relatively thicker cortex in 22q11DS.

Table 1:

Demographic Characteristics of the Sample

	22q11DS	TH	p-value
N	79	70	
Age*(years)*	22.1 (8.8) range 10.2 – 52.3	18.9 (3.5) range: 10.2 – 25.1	0.0046
Sex	42 Male (53%) 37 Female (46%)	38 Male (54%) 32 Female (46%)	0.8910
Race	65 White (82%) 9 AA (11%) 5 Other (6%)	50 White (71%) 15 AA (21%) 5 Other (7%)	0.2318
Deletion Length			
A-D	72 (91%)		
A-B	3 (4%)		
A-C	2 (3%)		
C-D	1 (1%)		
FISH only	1 (1%)		
Psychiatric Diagnoses			
Psychosis:	9 (11%)		
Schizophrenia	5 (6%)		
Schizoaffective Disorder	3 (4%)		
Psychotic Disorder NOS	1 (1%)		
Attention Deficit:	32 (40%)		
Anxiety Disorder:	43 (54%)		
Generalized Anxiety Disorder	17 (22%)		
Other anxiety disorders	26 (33%)		
Major Depressive Disorder:	22 (28%)		
Psychotropic Medications	44 (44%)		
SSRI	24 (30%)		
Antipsychotic	8 (10%)		
Stimulant	8 (10%)		
Antiepileptic	8 (10%)		
Unknown	4 (6%)		

Table 2:

Summary of group differences in cerebellar volumes (mm^3). Hypothesis tests assess mean group differences after adjusting for age, sex, race, and total brain volumes and after correcting for multiple testing. ROI-specific effect sizes (Cohen's d) are provided in Figure 3 and Table S1.

Left ROI		TD	22q11DS	F	p-value	Right ROI	TD	22q11DS	F	p-value
Anterior						**Anterior**				
Lobe	Mean	8823.83	7833.12	47.463	<0.0001	**Lobe**	8275.75	7057.69	88.27	<0.0001
	SD	1028.41	1025.85				995.72	866.06		
	SEM	15.12	12.99				14.64	10.96		
SPL	Mean	33278.83	27674.26	134.31	<0.0001	**SPL**	37834.73	31552.03	150.20	<0.0001
	SD	3177.50	3642.61				3594.83	4096.93		
	SEM	46.73	46.11				52.87	51.86		
IPL	Mean	14883.77	12303.44	139.67	<0.0001	**IPL**	12857.11	10860.98	95.66	<0.0001
	SD	1725.89	1594.72				1545.03	1316.93		
	SEM	25.38	20.19				22.72	16.67		
Lobules I/II	Mean	73.88	61.78	14.89	0.0002	**Lobules I/II**	96.80	81.02	22.07	<0.0001
	SD	20.39	15.84				24.38	17.19		
	SEM	0.30	0.20				0.36	0.22		
Lobule III	Mean	953.60	805.01	55.42	<0.0001	**Lobule III**	1060.04	866.00	73.60	<0.0001
	SD	129.32	132.98				145.54	136.99		
	SEM	1.90	1.68				2.14	1.73		
Lobule IV	Mean	2983.07	2681.60	19.54	<0.0001	**Lobule IV**	2312.40	2018.44	33.04	<0.0001
	SD	459.30	430.14				376.73	320.11		
	SEM	6.75	5.44				5.54	4.05		
Lobule V	Mean	4887.16	4346.51	47.49	<0.0001	**Lobule V**	4903.31	4173.26	83.10	<0.0001
	SD	569.39	577.23				613.63	524.09		
	SEM	8.37	7.31				9.02	6.63		
Lobule VI	Mean	9273.15	7864.90	88.07	<0.0001	**Lobule VI**	10135.19	8548.65	85.99	<0.0001
	SD	1079.80	1118.60				1240.64	1184.91		
	SEM	15.88	14.16				18.24	15.00		
Crus I	Mean	11725.35	9730.58	73.69	<0.0001	**Crus I**	12697.33	10847.62	66.11	<0.0001
	SD	1343.88	1597.03				1442.56	1622.81		
	SEM	19.76	20.22				21.21	20.54		
Crus II	Mean	8149.74	6718.33	84.46	<0.0001	**Crus II**	9519.20	7713.11	138.43	<0.0001
	SD	999.71	1025.15				1014.38	1191.68		
	SEM	14.70	12.98				14.92	15.08		
Lobule VIIB	Mean	4130.60	3360.46	93.16	<0.0001	**Lobule VIIB**	5483.02	4442.65	116.28	<0.0001
	SD	531.21	516.93				695.57	645.78		
	SEM	7.81	6.54				10.23	8.17		
Lobule VIIIA	Mean	6672.00	5429.93	139.43	<0.0001	**Lobule VIIIA**	5044.03	4134.08	94.93	<0.0001
	SD	815.62	799.24				692.73	639.38		

Left ROI		TD	22q11DS	F	p-value	Right ROI	TD	22q11DS	F	p-value
	SEM	11.99	10.12				10.19	8.09		
Lobule VIIIB	Mean	4136.13	3480.32	70.56	<0.0001	**Lobule VIIIB**	3833.13	3393.11	44.53	<0.0001
	SD	645.78	520.76				525.55	422.18		
	SEM	9.50	6.59				7.73	5.34		
Lobule IX	Mean	4075.64	3393.19	47.82	<0.0001	**Lobule IX**	3979.95	3333.79	48.84	<0.0001
	SD	662.45	508.75				618.76	465.23		
	SEM	9.74	6.44				9.10	5.89		
Lobule X	Mean	709.48	640.93	25.25	<0.0001	**Lobule X**	701.01	632.27	22.59	<0.0001
	SD	91.76	83.05				101.85	83.89		
	SEM	1.35	1.05				1.50	1.06		
White Matter	Mean	10133.51	8581.70	137.89	<0.0001	**White Matter**	9605.41	8114.96	132.90	<0.0001
	SD	878.02	1060.71				867.91	998.13		
	SEM	12.91	13.43				12.76	12.63		